unchanged. The more rapid increase in age at marriage that followed the antinatalist policies of 1970 produced a more pronounced reduction during the 1970s in the number of births that would have occurred with no change in age at marriage (and the same number of births at each duration for each couple). The policies of 1970 included measures to encourage limitation of marital fertility by the use of contraception and induced abortion, policies that culminated in the one-child norm introduced in 1979. The birth rate and the total age-specific fertility rate have not continued the decline of the 1970s, and the total second order birth rate has risen by more than 40% in the 1980s. We have shown that the total marital fertility rate by duration since first marriage did continue to decline at least until 1985, and that for married women the rate of bearing second and third children diminished (except for an upturn in the total second birth rate in 1986 and 1987). A major element in the undiminished or rising fertility calculated by age (as the TAFR) or for the whole population (as the birth rate) is the marriage boom that began when the government in 1980 relaxed the locally administered restrictions on marrying before an officially recommended age.

REFERENCES AND NOTES

1. China Population Information Centre, *Analysis on China's National One-per-Thousand-Population Fertility Sampling Survey* (New York, 1984).
2. A. J. Coale, *Soc. Forces* 67, 833 (1989).
3. ——— and Chen Sheng Li, Pap. East-West Pop. Inst. 104 (1987).
4. This value of TDFR1 implies that at the rates of first birth at each marriage duration in this decade, only 0.7% of married women would remain childless. This low a rate of sterility is inconsistent with data from some other populations. See, for example, J. Trussell and C. Wilson [*Pop. Stud.* **39**, 269 (1985)], where an estimate of 4.6% sterile is found from records in 14 English parishes from the mid-16th to the early 19th centuries. The 1982 census of China confirms a very low proportion childless: 1.47% among ever-married women 40 to 49. Actually, the average TDFR1 of 0.993 is slightly augmented by the decline in the mean duration of the interval between marriage and first birth in recent years. We have calculated this mean (for intervals of no more than 3 years) from 1970 to 1984 using data from the 1988 fertility survey. From 1976 to 1984 the average interval fell by about 1 month, or 0.083 years. Thus the average decrease in interval length was about 1% of a year annually, which would augment the TDFR by about 1%, just as the TMR is diminished by an increase in the mean age at marriage. Thus the TDFR1 with no change in the interval from marriage to first birth would be about 0.983, quite consistent with the 1.47% childless of ever-married women 40 to 49 reported in the 1982 census.
5. N. Luther, G. Feeney, and W. Zhang [*Pop. Stud.* **44**, 341 (1990)] come to similar conclusions on the basis of parity progression ratio.

Thermodynamics of Surface Morphology

ELLEN D. WILLIAMS AND N. C. BARTELT

Classical thermodynamic descriptions of surfaces treat surface orientation as a thermodynamic degree of freedom and thus allow for the possibility of reversible changes in surface morphology as a function of temperature or impurity concentration. The existence of these transitions has been confirmed experimentally. Advances in surface diffraction and imaging techniques now make it possible to characterize such transitions quantitatively in terms of the atomic structure, and particularly in terms of the behavior of steps on surfaces. Statistical mechanical models can be used to analyze the observations to determine the fundamental energetic parameters governing the observed thermodynamic behavior.

THE MORPHOLOGY OF SOLID SURFACES, THAT IS, THEIR structure on a scale of nanometers to micrometers, is the governing factor in a number of practical processes, including crystal growth, epitaxy, and etching. As a first step in developing a quantitative understanding of any of these processes, it is necessary to understand the equilibrium morphology of the surface. The profiles of two silicon surfaces [extracted from scanning tunneling microscopy (STM) data] (Fig. 1) illustrate the extent to which equilibrium thermodynamics can influence surface morphology (*1*, *2*). Both of these morphologies represent equilibrium configurations, with the difference being only the net crystallographic orientations of the surfaces. The stepped surface in Fig. 1A is defined by its net crystallographic orientation and can be considered a single thermodynamic phase. In contrast, the faceted profile in Fig. 1B contains regions of two distinct orientations and must be considered the coexistence of two thermodynamic phases.

The classical thermodynamic formalism for describing such surface morphologies and associated phase diagrams was put in place by Gibbs (*3*) and fully developed by Herring (*4*). Attempts to develop atomic models to calculate the surface free energies needed for thermodynamic prediction began as early as the 1920s (*5*), but little progress was made in extending them to nonzero temperature until the 1960s. Although recognized only in retrospect, Gruber and Mullins (*6*) developed the crucial insight that the thermal evolution of the surface free energy is governed by the wandering of steps (that is, linear boundaries across which the surface height changes by one or more atomic layers). Since then, statistical mechanical theories describing the surface free energy in terms of step behavior have been extensively developed (7). However, rigorous experimental tests of these theories only became possible in the 1980s, as more sophisticated surface preparation procedures, diffraction measurements, and new imaging techniques were developed.

In this article we show how experimental observations of steps can be used to test theoretical predictions about the orientational dependence of surface free energy, which governs the orientational phase diagrams of a surface. The extension of the underlying atomic models to provide a semiquantitative understanding of thermodynamic transitions observed on real surfaces is then illustrated by examples of reversible changes in surface morphology.

Theoretical Background

In this section we review how step properties are related to thermodynamic properties of surfaces. Crystallographic orientations of high symmetry (low–Miller index surfaces) will generally repre-

---

The authors are in the Department of Physics and the Institute for Physical Science and Technology, University of Maryland, College Park, MD 20742.

sent local minima in the surface free energy. At low temperature these minima are in the form of cusps, and the associated surfaces are called, by definition, facets. At small angles of misorientation ϕ from such surfaces, one can calculate the surface free energy by considering the surface as consisting of terraces of the low-index orientation separated by steps of atomic-layer height. If the step density is low enough, the variation of the surface free energy (per projected area in the low-index plane) with angle ϕ and temperature T is governed by (*8, 9*)

$$f(\phi,T) = f_0(T) + \frac{\eta(T)}{h}|\tan\phi| + \frac{B(T)}{a_\| h^3}|\tan\phi|^3 \qquad (1)$$

The terms in Eq. 1 can be understood by referring to Fig. 2, which shows a Monte Carlo simulation of a stepped surface based on a simple lattice model. The first term $f_0(T)$ is the surface energy per unit area of the low-index surface. The terraces between the steps in Fig. 2 have the microscopic orientation of the low-index surface. Because $\tan\phi$ is proportional to the step density, the coefficient of the second term, $\eta(T)$, is the free energy per unit length for forming an isolated single-layer-height step. The thermal dependence of this term comes from the possibility of exciting kinks at the edges of the steps. The formation of the kinks allows the step to wander, increasing the entropy and thus decreasing the free energy for step formation. At low temperatures, this free energy change can be determined from the partition function for formation of independent kinks of length $a_\perp$ costing energy ϵ. The resulting step formation energy at low temperature for the kink geometry of Fig. 2 is

$$\eta(T) = \eta(0) - \frac{2kT}{a_\|}\exp(-\epsilon/kT) \qquad (2)$$

where k is Boltzmann's constant. At high temperatures, when excitations on terraces occur, it is known that the step formation energy can eventually disappear according to

$$\eta(T) \approx \exp\left(\frac{-c}{\sqrt{T_R - T}}\right) \qquad (3)$$

where c is a constant, leading to the roughening transition at T_R of the low-index facet (*7*). For the subsequent discussion, we assume that the surfaces of interest are well below this roughening temperature. We also neglect discussion of failures of the lattice model that occur near the bulk melting temperature, leading to the interesting phenomenon of surface premelting (*10*).

The third term in Eq. 1 is due to interactions between the steps. B is the free energy coefficient attributable to step interaction. Much theoretical work in the past decade (*8, 9, 11*) has revealed [as anticipated by Gruber and Mullins (*6*)] that, in addition to changing the formation energy for an isolated step, the step wandering contributes to this interaction term, even in the absence of any energetic interactions between the steps. This occurs because the wandering of a step will be limited by its inability to cross neighboring steps. The resulting decrease in the entropy of wandering leads to an effective entropic repulsion between steps, which can be illustrated by considering the model case of a wandering step trapped between two fixed walls at positions $x = \pm\ell$. The step has the largest configurational entropy when it is midway between the walls, leading to a peaked position probability function at low temperature

$$P(x,\ell) = (1/\ell)\cos^2(\pi x/2\ell) \qquad (4)$$

even though there is no energetic interaction between the step and the walls (*6, 12*). [The case for which all steps are wandering simultaneously can be solved numerically, with a result showing that Eq. 4 is adequate for data analysis when the kink density is low

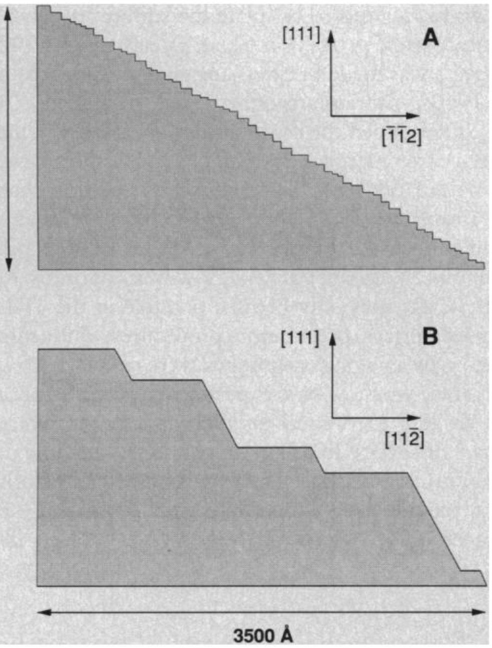

Fig. 1. Surface profiles of two silicon surfaces, each misoriented from the [111] direction by 4°, but along different azimuthal directions (*1, 2*). (**A**) Misorientation azimuth [$\bar{1}\bar{1}2$]; (**B**) misorientation azimuth [$11\bar{2}$]. Data were compiled by "tiling" adjacent atomic-resolution STM scans to form a composite profile covering a cross section 4000 Å wide.

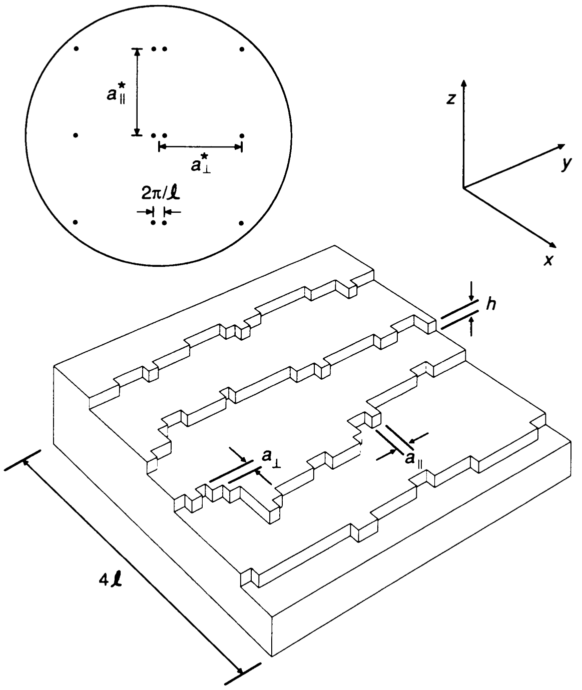

Fig. 2. Result of a Monte Carlo calculation of a stepped surface in thermal equilibrium. The model used is a cubic lattice with near-neighbor interactions, with $a_\|$ and $a_\perp$ defined. The boundary conditions were set to give a misorientation angle $\tan\phi = h/\ell$ with $\ell = 8a_\perp$ and $h = a_\perp$. **Inset:** Representative LEED pattern showing "unsplit" diffraction beams at in-phase scattering conditions (path length difference for scattering off of adjacent terraces equals integral number of wavelengths), and beams at out-of-phase conditions with splitting direction perpendicular to the average step-edge direction, and magnitude inversely proportional to the average step separation.

(*12*).] The effect of this entropic interaction on the free energy is known exactly in the limit of small kink and step densities

$$B(T) = g(T), \text{ where } g(T) = \frac{\pi^2}{12} kTb^2(T) \qquad (5)$$

and the step "diffusivity" $b^2(T)$ is the mean-squared displacement of an isolated step perpendicular to the step edge (*13*). As one would expect, the value of b^2 depends on the ease of kink formation as $e^{-\epsilon/kT}$.

If there are also energetic interactions between the steps, these will affect only the $\tan^3 \phi$ and higher order terms as long as the interaction falls off at least as rapidly as x^{-2} (*8*). For the specific case of energetic interactions of the form $U(x) = A/x^2$ [where $U(x)$ is the potential energy per unit step length], at low temperature the free energy due to the step interaction is (*8, 14*)

$$B(T) = \frac{g(T)}{4} \left\{ 1 + \left[1 + \frac{2\pi^2 A a_\|}{3\, g(T)} \right]^{1/2} \right\}^2 \qquad (6)$$

As in the case of the entropic interactions, a small kink formation energy allows the steps to wander close to one another and results in a large free energy cost due to energetic step interactions.

In summary, the fundamental behavior of the surface free energy is governed by four parameters: the free energy of the facet, the step formation energy, the kink formation energy, and the energetic interactions between steps. As we will show, this small set of parameters can lead to a remarkable diversity of surface morphologies.

Experimental Background

Elegant tests of Eq. 1 have been performed by direct measurement of the shape of carefully equilibrated macroscopic crystals of helium and of metals (*15–17*). In contrast, it is possible to test the thermodynamics of macroscopic surfaces (which are by no stretch of the imagination part of a real equilibrium crystal) by measurement of the step behavior. Surfaces with a controlled step density are prepared by mechanical preparation of the net surface orientation at a fixed angle with respect to a low-index plane. In both types of experiments, equilibration of the surface structure requires careful attention. Any surface impurities can change the surface free energy or act as pinning sites that alter the step structure. For solids with low vapor pressures, equilibration of the surface structure at temperatures of interest may only be possible by surface diffusion, requiring prolonged annealing under ultrahigh vacuum conditions to maintain cleanliness. At low temperatures, surface diffusion may be so slow that the equilibrium configuration of a higher temperature is frozen in.

The step structure can be measured through the complementary combination of diffraction and direct-imaging techniques. Diffraction provides information on the short- and long-range order and on the representative average structure. Direct imaging allows statistical deviations from the average behavior to be assessed. Low-energy electron diffraction (LEED) is most commonly used to determine step structure because of its surface sensitivity and the ease with which the wavelength of the probing electrons can be varied (*18*) [although other techniques such as He diffraction can also be used effectively (*19, 20*)]. Data acquisition rates with LEED are rapid enough that monitoring thermal transitions of surface step structure is limited by the equilibration rate [less than 0.5°C per second for Si(111) at 800°C]. The characteristics of LEED patterns for stepped surfaces are illustrated schematically in the inset of Fig. 2. The step height, direction, and spacing can be determined from the momentum transfer, the direction, and the magnitude of the splitting of the diffraction beams, respectively. A great deal of disorder in the step configurations is possible without loss of observable beam splitting. However, the statistical variations in the step separations due to step wandering do give rise to a distinctive signature in the diffraction line shapes. Analogous to domain-wall structures, the wandering steps cause a power-law variation of the line shape (*12, 21*). Quantitative analysis of such diffraction line shapes is difficult. However, the high resolution possible with development of surface x-ray diffraction should provide some access to this information (*22, 23*). Line-shape analysis is also possible with He diffraction, although the effect of inelastic scattering must be treated with care (*24*). Failures of the lattice model can be detected very effectively via ion-scattering (*10*).

The statistical behavior of surface step structure can be more directly probed by imaging techniques. The wandering of surface steps can be imaged with moderate (on the order of 100 Å) resolution with reflection high-energy electron microscopy (REM) (*25*), low-energy electron microscopy (LEEM) (*26*), and, in special cases, transmission electron microscopy (TEM) (*27*). The first two of these techniques are especially useful, as they allow imaging at elevated temperature and in real time. Although such analysis has not yet been performed, the images of wandering steps obtained with these techniques can be used to determine the mean-squared length of the kinks (assuming the kinks do not interact) through the diffusivity of the step edge position

$$b^2 = \langle [x(0) - x(y)]^2 \rangle \frac{a_\|}{y} \qquad (7)$$

where the coordinate system is as defined in Fig. 2. More detailed information about the atomic and kink structure of steps can be obtained with STM (*28*). This technique allows atomic-resolution imaging with a limited field of view and with limited time resolution. The approximate imaging time is several minutes for an atomic

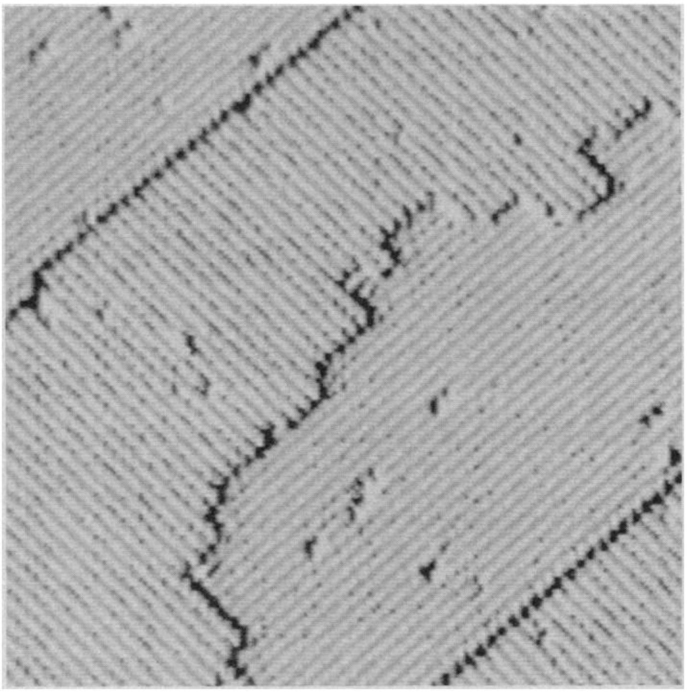

Fig. 3. A 500 Å by 500 Å image of an Si(100) surface misoriented by 0.3° toward the $[1\underline{1}0]$ direction, measured by Swartzentruber *et al.* (*30*). Step height is 1.4 Å and mean terrace width is 260 Å. Adjacent terraces have alternating directions of dimerization of the surface atoms, visible as parallel lines (separation, 7.7 Å) in the image. As a result, the kink-formation energy on alternate steps is different.

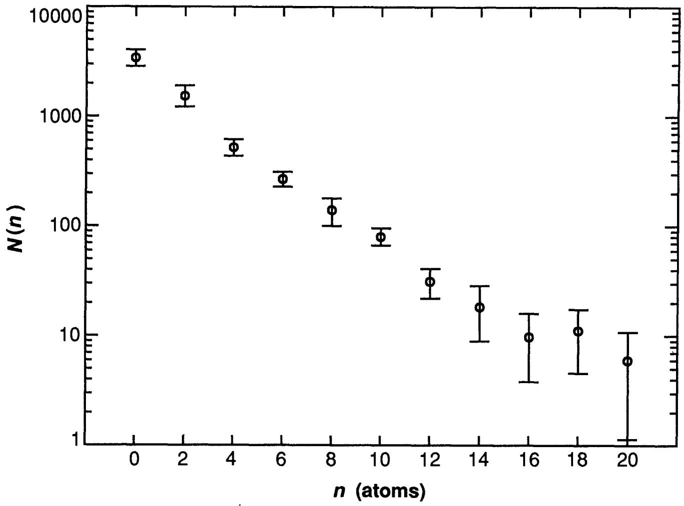

Fig. 4. The kink-length distribution on the alternate "rough" steps on vicinal Si(100). The measured number of kinks of length *n*, $N(n)$ is plotted versus *n*. The value at $n = 0$ is the number of sites at which there is no kink. The error bars are given as the sum of the statistical error and a systematic counting error determined by counting an identical data set several times. Data compiled and analyzed by Swartzentruber *et al.* (*30*), from a large number of STM images such as those shown in Fig. 3.

resolution scan over an area of 500 Å by 500 Å. In order to obtain statistically significant data, large numbers of such areas must be sampled and the results must be carefully cross-checked with a surface-averaging technique such as LEED. In addition, STM measurements are typically limited to temperatures not much above room temperature, which are below the equilibration temperature for many materials (*29*). Thus, the room-temperature STM images that we show for Si represent structures equilibrated at a higher temperature (typically 500° to 600°C).

The application of combinations of these techniques to measurement of step configurations now makes it possible to test the theories outlined above directly. Such measurements allow quantitative determination of at least some of the parameters governing step behavior. In addition, it is also possible to characterize more complex transitions involving surface morphology that occur in real materials.

Experimental Confirmation of Step Wandering

Particularly beautiful quantitative studies of step wandering have been performed on vicinal (stepped) Si(100) surfaces (*30–32*). The crystal structure of Si allows two energetically different types of single-layer-height steps to form on the (100) surface. The kink energies on these two step types are quite different, leading to markedly different amounts of step wandering. This is illustrated in Fig. 3, in an STM image by Swartzentruber *et al.* for a surface equilibrated at approximately 600°C (*30*). Alternating steps are nearly straight, leading to a structure similar to the simple Gruber-Mullins (*6*) model of a wandering step trapped between two walls. Swartzentruber *et al.* have analyzed the kink density along the wandering step edges, using a Boltzmann probability for independent kink excitations

$$N(n) = 2N(0) \exp\left[-\epsilon(n)/kT\right] \qquad (8)$$

where $\epsilon(n)$ is the energy of a kink of depth *n* spacings and $N(n)$ is the number of kinks observed at that depth. The results of this measurement are illustrated in Fig. 4. Analysis of these results with the use of Eq. 8 show that $\epsilon(n)$ deviates slightly from the value $n\epsilon$ expected from a simple lattice model according to

$$\epsilon(n) = n\epsilon + C \qquad (9)$$

(where C is a constant) and gives a kink energy of $\epsilon/kT = 0.37 \pm 0.03$ atom^{-1} (*30*).

Data from large numbers of images such as that in Fig. 3 can be compiled to test Eqs. 4 through 7 and to measure the form and strength of any energetic interactions between steps. Such an analysis has been peformed for step wandering on Si(111) from the measured position distribution function of the steps, shown in Fig. 5 (*33*). The measured distribution is significantly narrower than the calculated distribution for freely wandering steps, indicating that there is a repulsive energetic interaction acting between steps. One can obtain good estimates of the expected narrowing of the distribution due to energetic interactions by considering the simple trapped-step model. Restricting the step to a narrower range of positions, $w < \ell$, will increase the free energy by decreasing the entropy of wandering, at the same time that it decreases the free energy by reducing the energetic repulsion. If the potential energy per unit length of step is $U(x)$, then the modified step position distribution becomes (*12*)

$$P(x,\ell) = \frac{1}{w\sqrt{(2\pi)}} \exp\left(-x^2/2w^2\right) \qquad (10)$$

with

$$w(x,\ell) = \left[\frac{kTb^2\,(T)}{8U''(\ell)a_{\parallel}}\right]^{1/4} \qquad (11)$$

For the Si(111) step distributions measured with two different step separations, the data give $w = 36$ Å for $\ell = 146$ Å, and $w = 21$ Å for $\ell = 79$ Å. These values indicate a direct proportionality between w and ℓ, and thus a form for $U(x)$ of A/x^2, that is consistent with either an elastic or a dipole origin for the energetic interaction. Using Eqs. 5 and 11 and the measured value of $w/\ell \approx 0.26$ allows us to determine that $A/g \approx 6/a_{\parallel}$. This will increase the magnitude of the step interaction term in the free energy by over a factor of 10,

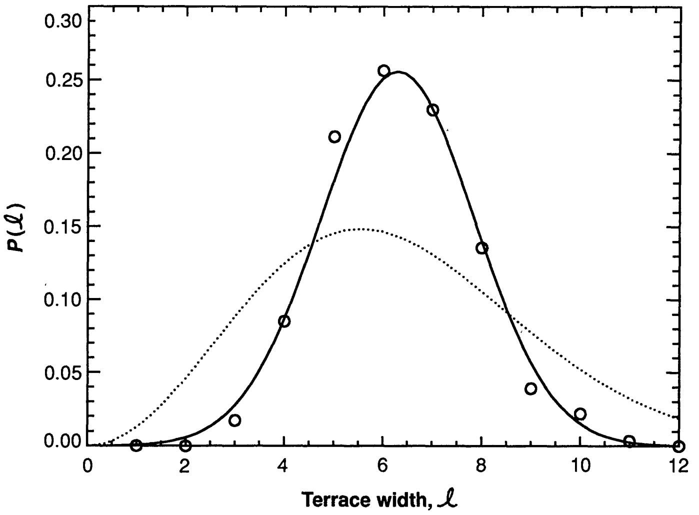

Fig. 5. Terrace-width distribution for Si(111) surfaces misoriented 1.2° toward the $[2\bar{1}\bar{1}]$ direction. $P(\ell)$ is the probability of occurrence of a terrace of width in units of 1/2 the 7 × 7 unit cell (23 Å) in the $[2\bar{1}\bar{1}]$ direction. Only terraces bounded by single-layer-height steps are included in the data. Open circles show the data compiled from observations of 151 terraces. The dotted line is the calculated curve for freely wandering steps, the solid curve is calculated from Eq. 10 with $w = 36$ Å. Similar data were also compiled for 482 terraces on a sample misoriented by 2.3° (*1*).

Table 1. The relative fraction of triple- and single-height steps observed on Si(111) surfaces misoriented toward the $[2\bar{1}\bar{1}]$ direction, as a function of the misorientation angle ϕ (*1*). The average step separation ℓ_{single}, which would occur if all steps were single-height, is compared with the average ℓ_{mix} for the observed fraction of triple-layer steps.

ϕ (deg)	Fraction of triples	ℓ_{single} (Å)	ℓ_{mix} (Å)
1.2	0.08	138	161
2.3	0.17	72	96
3.8	0.33	47	78
6	0.75	30	75

compared with freely wandering steps. A similar analysis of data for varying step densities (*32, 34*) can be used to test the rather specific predictions that have been made for step interactions on Si(100) (*35*).

The examples discussed above indicate the type of measurements that can now be performed to determine the quantitative parameters governing step structure. An ideal series of measurements would involve a range of sample misorientations corresponding to step separations from thousands of angstroms to tens of angstroms to determine both the kink energy and the step interactions. Measurements over a wide range of temperature would be performed with the use of both LEED and either REM or LEEM, and details of the atomic structure of the steps would be measured near room temperature with STM. As discussed in the following two sections, such studies can also be used to measure the phase transitions in surface morphology that can result from the orientational variations in the surface free energy.

Step-Height Changes

Changes in overall surface morphology involve rearrangements in the step structure. One obvious possible step structural transition involves changes in the height of the step, an example being halving the number of steps while preserving the net orientation by doubling their height and mean separation. The possibility of such transitions is not apparent in Eq. 1, which shows only the effect of orientational variation. However, it is easy to imagine how such transitions can occur if we consider simple lattice models. We can distinguish two generic cases of step-height variation: one in which an isolated multilayer step has a larger step formation energy than a single-layer step, and one in which an isolated multilayer step has a lower step formation energy. The basic physics of the first case can be illustrated by consideration of a cubic lattice with only near-neighbor interactions. For this model, the step formation energy at $T = 0$ for an n-layer step is n times that for a single-layer step. At nonzero temperature, entropy (see Eq. 2) causes the single-layer step to be favored, as there is no energy cost for the breakup of an isolated multilayer step into single-layer steps. However, at larger step densities, the step interaction term will be smaller for the multilayer steps because of their larger step separation and larger kink energy. Thus, one might expect a continuous increase in the concentration of multilayer steps with angle of misorientation, as the step interaction term becomes comparable in magnitude to the step formation term in the free energy. Another possibility is a purely first-order phase transition between two phases with purely single and multilayer height configurations (*35a*). This orientational variation will clearly depend on the relative step formation energies and kink formation energies for the single and multilayer height steps, as well as some configurational entropy of mixing. No calculations have specifically addressed the issue of such mixed step-height configurations, although at moderate temperatures and step densities such configuration may result in much rougher surfaces than would be the case when only single-height steps are present.

A possible example of this type of behavior occurs for steps on

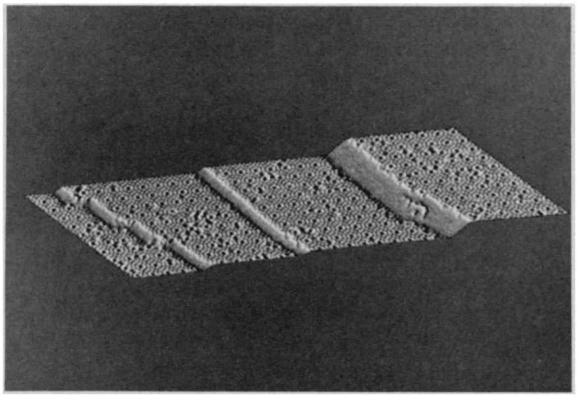

Fig. 6. A 200 Å by 800 Å STM image of an Si(111) surface misoriented 1.2° toward the $[2\bar{1}\bar{1}]$ direction, shown as a shaded surface. One triple-layer and two single-layer height steps are visible. Kinks along the step edges follow the 7 × 7 unit cell.

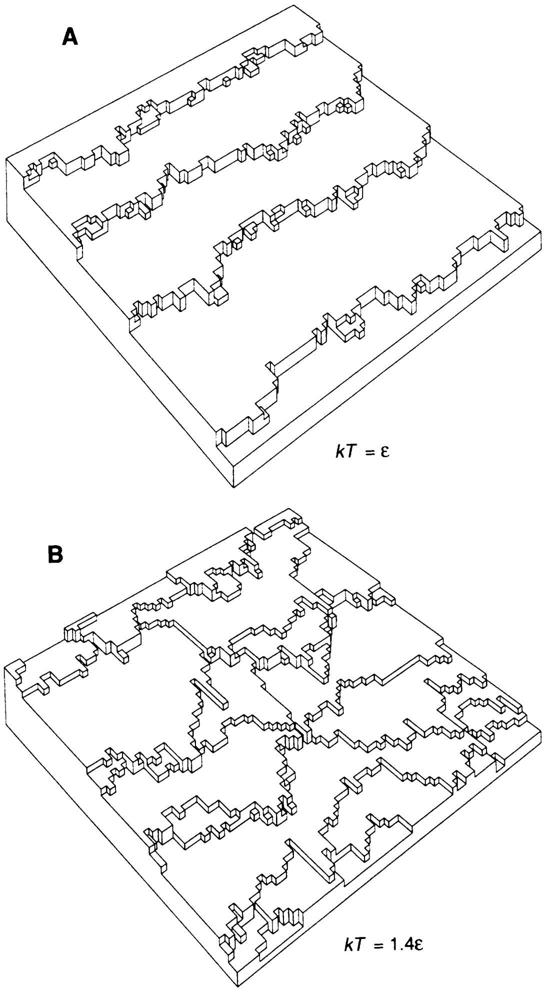

Fig. 7. Monte Carlo simulations of a step-doubling transition. (**A**) A relatively low-T configuration composed of predominately double-layer height steps. (T is equal to the kink energy, ϵ, of single-layer-height steps, with the kink energy of single-layer steps equal to that of double-layer steps.) (**B**) A high-T ($T = 1.4\epsilon$) configuration of mostly single-layer-height steps.

Si(111) misoriented toward the $[2\bar{1}\bar{1}]$ direction, where there is a strong repulsive interaction between steps. An experimental result, an image of a sample misoriented by 1.2°, is illustrated in Fig. 6 (*1*). Both single- and triple-layer steps appear on the surface in an apparently random mixture. For the small-step density the steps are primarily single height, whereas for increasing step density the steps are primarily triple height (*1, 36*), a trend confirmed by a statistical analysis of many such STM images (Table 1). Profiles of the surfaces involving hundreds of steps over distances of approximately 5000 Å show a mixture of single-layer, triple-layer, and occasional six-layer-high steps (*1*). (Other step heights, which are not observed, presumably have much larger step formation energies.) An analysis of the height-height correlation function for the 6°-misoriented surface shows that it is significantly rougher than the expectation for a surface containing only single-layer height steps. The rapid increase in triple-layer steps with step density shows that the strong repulsion between singles becomes comparable to the difference in single- and triple-height step formation energies at step separations around 100 Å.

The second type of step-height transition, in which an isolated multilayer step costs less energy than a single-layer step, does not arise naturally in simple lattice models. However, it is easy to envision a real system where the vagaries of bond formation at the step edge favor a specific step height. Such a situation was predicted by Chui and Weeks (*37*) to lead to a thermal transition in step height analogous to a wetting transition in fluid interfaces. This might occur when double-height steps have a lower step formation energy than single-height steps (and all other step heights are much more costly). Then the double-height steps would be stable at low temperatures, and disorder to singles at high temperatures where the entropic wandering (Eq. 2) of the single-height steps becomes important. A simulation of such a transition is shown in Fig. 7, A and B, for a case in which two single steps cost twice the energy of a double-height step. The transition is second-order and seems to fall in the Ising universality class. Although there have been many reports of such step-height phase transitions (*38–40*), no detailed comparison of the experimental results with theory has yet been made.

Faceting

The most profound changes in surface morphology occur when steps coalesce to form facets. When such changes can be demonstrated experimentally to be reversible, it is reasonable to describe them in terms of equilibrium thermodynamics. Herring first quantified the requirements on the variation of the surface free energy with orientation for such a phase separation to occur (*4*). The stability of any given surface orientation on such a crystal is governed by a convexity requirement on the surface free energy as a function of orientation. A surface with orientation defined by normal $\hat{n}_0$ will only be stable if the total free energy cannot be lowered by creating a zigzag (faceted) structure of planes of different orientation $\hat{n}_i$. This requirement is quantified by the two equations

$$A_0\gamma(\hat{n}_0) < \sum_i A_i\gamma_i(\hat{n}_i) \tag{12}$$

and

$$A_0\hat{n}_0 = \sum_i A_i\hat{n}_i \tag{13}$$

where $\gamma(\hat{n}_i)$ are the free energies per unit area of orientations $\hat{n}_i$, and A_i are the areas of the surfaces of orientations $\hat{n}_i$ (*41*). In simple lattice models, a stepped surface can phase-separate (at low enough temperature) only into neighboring low-index orientations. In real crystalline materials, more complex interactions allow for a greater variety of transitions (*42*), such as phase separation between a facet and a surface of different step density or between two regions of different step density. One mechanism for such behavior is a phase transition on the surface of a facet. Real surfaces often lower their surface free energy by formation of a new (reconstructed) structure much different from the bulk termination of the solid lattice. [On Si(111) the reconstruction of 7 × 7 periodicity disorders in a first-order transition to a structure of 1 × 1 periodicity at approximately 850°C.]

We can qualitatively understand how the first-order phase transition between two such surface structures can lead to orientational phase separation by using Eq. 1 to calculate free energy curves for the two structures (*43*). At the transition temperature, the free energies of the reconstructed and unreconstructed facets must be the same. However, the step formation and kink formation energies of the two structures will generally be different. As one example, we can choose both the kink and step formation energies much larger for the phase stable at low temperature (other choices will lead to different phase diagrams), leading to the two curves shown in Fig. 8A. As the temperature decreases, the free energy of the low-T phase drops relative to that of the high-T phase, with the result that the net free-energy curve is no longer convex, as shown in Fig. 8B. A phase separation then must occur between the low-index facet and a region of greater step density, as indicated by the dashed line (*16, 44*). The relative areas of the two phases are governed by the lever rule (Eqs. 12 and 13), with the angle of the stepped phase given by

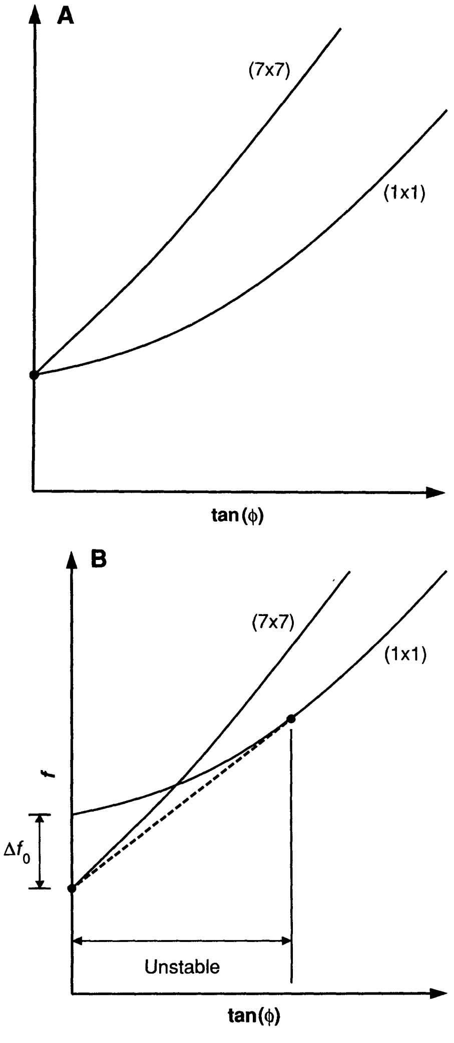

Fig. 8. Schematic evolution of free-energy curves with temperature of the type that leads to reversible faceting of Si(111). The unreconstructed "(1 × 1)" phase and the "(7 × 7)" phase are envisioned to have different dependences of f on ϕ. At the temperature of the 1 × 1 to 7 × 7 transition (T_c) on the (111) (ϕ = 0) surface, these two curves cross. (**A**) Plot of f versus tan ϕ at T_c; (**B**) plot of f versus tan ϕ below T_c. Below T_c the intersection of the two curves leads to a region of unstable (faceted) surfaces at small ϕ.

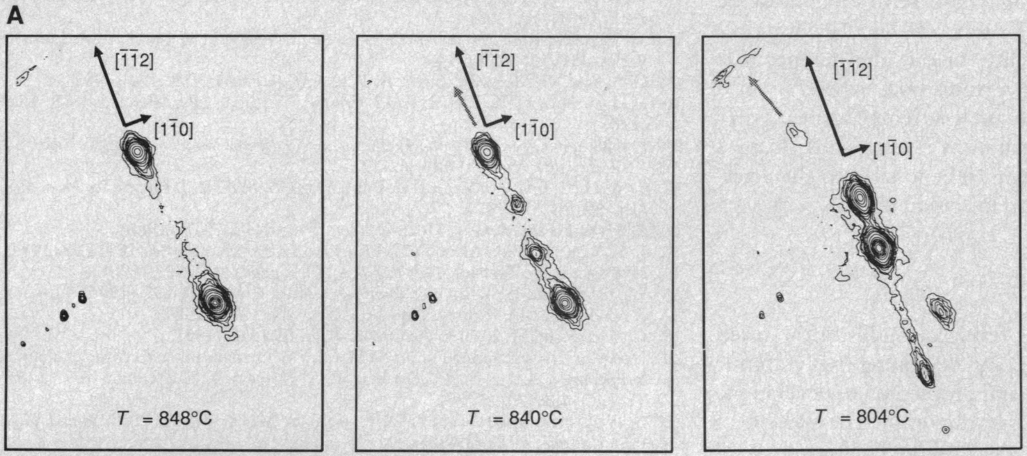

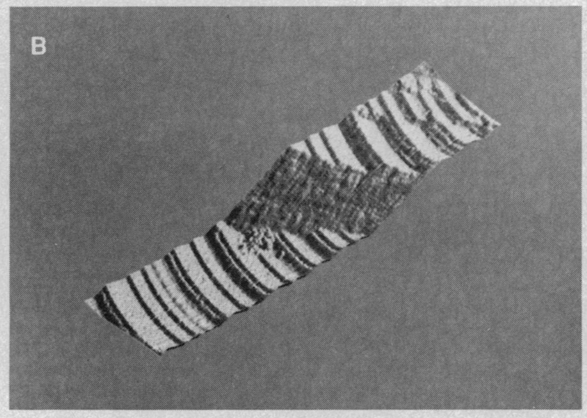

Fig. 9. Data from an Si(111) sample misoriented by 6° toward a direction 10° away from the $[2\bar{1}\bar{1}]$ azimuth. (**A**) Contour plots of the LEED intensity near the specular beam at an out-of phase condition for both single- and triple-layer height steps; 848°C is above the reconstruction transition, 840°C is just below the reconstruction transition, and 804°C is well below the reconstruction transition. (**B**) A 200 Å by 800 Å STM image of the surface structure at room temperature showing two phases: a stepped surface of 6° misorientation toward the $[2\bar{1}\bar{1}]$ azimuth (note the absence of kinks at step edges), and an azimuthally rotated surface with $\phi \approx 20°$ and $\theta \approx 40°$.

$$\Delta f_0 = \frac{2B(T)}{a_{\|}h^3}\tan^3\phi \tag{14}$$

The angle of the stepped phase will increase continuously in this scenario as Δf_0 increases with decreasing temperature, allowing either Δf_0 or the interaction term $B(T)$ to be determined if the other is known (*43*). Such a phase diagram has been observed experimentally with LEED for Si(111) misoriented toward the $[\bar{2}11]$ direction (*2, 43, 45, 46*). We can expect analogous behavior to occur when surface free energies are changed by chemical adsorption, leading to the well-known phenomenon of impurity-induced faceting (*40, 47, 48*).

The example above illustrates faceting along a fixed azimuth. Virtually all of the statistical mechanical calculations are limited to misorientations along a fixed, implicitly high-symmetry direction. However, transitions involving azimuthal variations are also possible and are potentially very interesting (*4, 42*). We can consider the effect of introducing a small azimuthal miscut to a step staircase along a high-symmetry direction. The effect will be to rotate the step edge direction by introducing a fixed kink density along the step edge. Such a large kink density will only be stable if the surface cannot lower its free energy by faceting. An example of a reversible azimuthal faceting transition in such a case is shown in the LEED data of Fig. 9A for vicinal Si(111) (*49*). At high temperature, there is a single-step orientation consistent with the macroscopic surface orientation. Upon cooling, a second set of diffraction beams appears corresponding to a step staircase along the high-symmetry $[2\bar{1}\bar{1}]$ direction, while the original beams rotate to increased azimuthal angle. The relative changes in orientation are consistent with the lever rule requirement for fixed macroscopic orientation. The result clearly suggests the expulsion of the kinks from the step edges due to a large kink energy in the presence of the reconstruction. This is confirmed by STM images such as Fig. 9B, which shows straight steps with low kink density along the $[2\bar{1}\bar{1}]$ direction, with intervening 7×7 reconstructed terraces, and an azimuthally rotated facet of much steeper polar angle. This transition is driven by the formation of the 7×7 reconstruction on the (111) surface. Thus, we can understand the phase separation as due to a loss of convexity when the free-energy curves for the reconstructed and unreconstructed structures intersect.

Observations of reversible faceting transitions can be understood at least qualitatively in terms of the simple parameter set governing step behavior and the surface free energy, providing a satisfying illustration of the connection between atomic models and classical thermodynamics for these problems. The thermodynamic information about the orientational stability of surfaces that is obtained from such observations can be summarized in the form of phase diagrams, as shown in Fig. 10 for surfaces near Si(111). In these diagrams, the radial distance from the point representing the (111) orientation is proportional to the tangent of the polar angle. In this

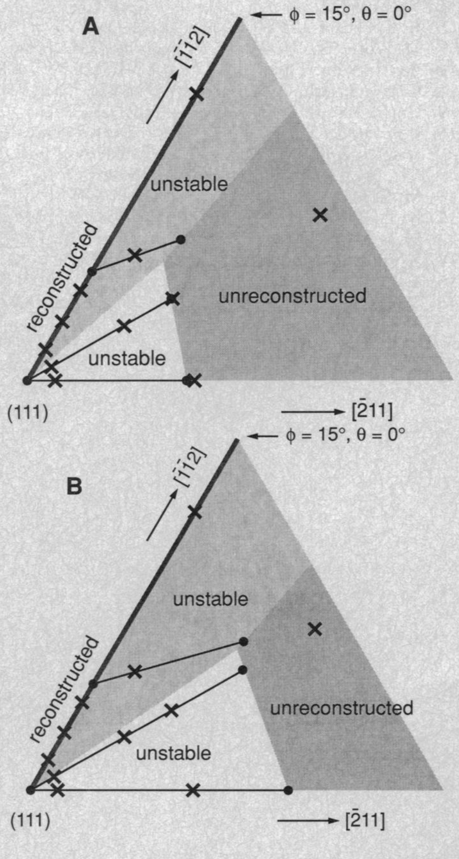

Fig. 10. Phase diagrams at (**A**) $T =$ 820°C and (**B**) $T =$ 800°C showing the observations from vicinal Si(111) surfaces (*49*). The diagrams are polar plots of tan ϕ. Crosses mark the studied surface orientations, filled circles mark the observed boundaries of the coexistence regions, and the solid lines are the associated tie lines. In the unshaded unstable region, surfaces undergo faceting between surfaces of different polar but fixed azimuthal angles (an example is shown in Fig. 1B). In the shaded unstable regions the faceting includes a change in azimuthal angle as well, as illustrated in Fig. 9.

representation, the tie bars indicating phase separation must be straight lines according to Eq. 13. The series of Fig. 10, A and B, shows the evolution of step stability below the temperature (≈850°C) of the 7 × 7 reconstructive transition, where stepped surfaces of all orientations are stable, at low temperatures where both azimuthal and polar phase separation occur. Thus, from a relatively small number of measurements, it is possible to characterize the stability of a wide range of surface orientations.

Conclusions

The organization of this article has reversed the historical development of surface thermodynamics, by beginning with atomic predictions for the surface free energy and proceeding to develop the types of orientational phase diagrams that can result. The purpose of this reversal was to allow a strong emphasis on the important role of steps in determining the surface free energy, and on the recent experimental advances that now make it possible to characterize step behavior very accurately. The significance of these advances extends beyond the equilibrium properties discussed here, as steps are the fundamental units in the surface mass transport required for morphological phase transitions, and for kinetically limited processes such as growth. Thus, the experimental and related theoretical capabilities for dealing with the equilibrium properties of steps, which have been reviewed here, will find extensive applications in studies of nonequilibrium phenomena as well (*50–53*).

REFERENCES AND NOTES

1. X. S. Wang, thesis, Department of Physics, University of Maryland, College Park (1990).
2. R. Gomez, thesis, Department of Physics, University of Maryland, College Park (1990).
3. *The Collected Works of J. Willard Gibbs* (Yale Univ. Press, New Haven, CT, 1957), vol. 1.
4. C. Herring, *Phys. Rev.* **82**, 87 (1951).
5. W. Kossel, *Nachr. Ges. Wiss. Göttingen* **K1**, 135 (1927).
6. E. E. Gruber and W. W. Mullins, *J. Phys. Chem. Solids* **28**, 875 (1967).
7. M. Wortis, in *Chemistry and Physics of Solid Surfaces*, R. Vanselow and R. Howe, Eds. (Springer, Berlin, 1988), vol. VII, pp. 367–405, and references therein.
8. C. Jayaprakash, C. Rottman, W. F. Saam, *Phys. Rev. B* **30**, 6549 (1984).
9. C. Jayaprakash, W. F. Saam, S. Teitel, *Phys. Rev. Lett.* **50**, 2017 (1983).
10. J. F. van der Veen, B. Pluis, A. W. Denier van der Gon, in *Chemistry and Physics of Solid Surfaces*, R. Vanselow and R. Howe, Eds. (Springer, Berlin, 1988), vol. VII, pp. 455–490, and references therein.
11. M. E. Fisher, *J. Stat. Phys.* **34**, 667 (1984).
12. N. C. Bartelt, T. L. Einstein, E. D. Williams, *Surf. Sci.*, in press.
13. M. E. Fisher and D. S. Fisher, *Phys. Rev. B* **24**, 3192 (1982).
14. B. Sutherland, *Phys. Rev. A* **4**, 2019 (1971).
15. Y. Carmi, S. G. Lipson, E. Polturak, *Phys. Rev. B* **36**, 1894 (1987).
16. J. E. Métois and J. C. Heyraud, *Ultramicroscopy* **31**, 73 (1989), and references therein.
17. M. Drechsler, in *Surface Mobilities on Solid Materials*, V. T. Binh, Ed. (Plenum, New York, 1981), pp. 405–457.
18. M. Henzler, in *Electron Spectroscopy for Surface Analysis*, H. Ibach, Ed. (Springer, Berlin, 1977), pp. 117–149.
19. G. Comsa, G. Mechtersheimer, B. Poelsema, *Surf. Sci.* **119**, 172 (1982).
20. M. Den Nijs, E. K. Riedel, E. H. Conrad, T. Engel, *Phys. Rev. Lett.* **55**, 1689 (1985).
21. J. Villain, in *Ordering in Strongly Fluctuating Condensed Matter Systems*, T. Riste, Ed. (Plenum, New York, 1980), pp. 221–259.
22. G. A. Held, J. L. Gordon-Sweet, P. M. Horn, A. Mak, R. J. Birgeneau, *Phys. Rev. Lett.* **59**, 2075 (1987).
23. B. M. Ocko and S. G. J. Mochrie, *Phys. Rev. B* **38**, 7378 (1988).
24. E. H. Conrad, L. R. Allen, D. L. Blanchard, T. Engel, *Surf. Sci.* **184**, 227 (1987).
25. N. Osakabe, Y. Tanishiro, K. Yagi, G. Honjo, *ibid.* **109**, 353 (1981).
26. W. Telieps and E. Bauer, *Ber. Bunsenges. Phys. Chem.* **90**, 197 (1986).
27. R. T. Tung and F. Schrey, *Phys. Rev. Lett.* **63**, 1277 (1989).
28. G. Binnig and H. Rohrer, *Rev. Mod. Phys.* **59**, 615 (1987).
29. However, for an example of an STM study of changes in surface morphology at temperature, see J. W. M. Frenken, R. J. Hamers, J. E. Demuth, *J. Vac. Sci. Technol. A* **8**, 293 (1990).
30. B. S. Swartzentruber, Y.-W. Mo, R. Kariotis, M. G. Lagally, M. B. Webb, *Phys. Rev. Lett.* **65**, 1913 (1990).
31. D. Dijkkamp, A. J. Hoeven, E. J. Van Loenen, J. M. Lenssinck, J. Dieleman, *Appl. Phys. Lett.* **56**, 39 (1990).
32. G. P. Kochanski, *Phys. Rev. B* **41**, 12334 (1990).
33. X.-S. Wang, J. L. Goldberg, N. C. Bartelt, T. L. Einstein, E. D. Williams, *Phys. Rev. Lett.* **65**, 2430 (1990).
34. R. Kariotis, B. S. Swartzentruber, M. G. Lagally, *J. Appl. Phys.* **67**, 2848 (1990).
35. O. L. Alerhand *et al.*, *Phys. Rev. Lett.* **64**, 2406 (1990).

35a. N. C. Bartelt, T. L. Einstein, C. Rottman, *Phys. Rev. Lett.*, in press; C. C. Umbach, M. E. Keefe, J. M. Blakely, *J. Vac. Sci. Technol. A*, in press.

36. R. J. Phaneuf and E. D. Williams, *Phys. Rev. B* **41**, 2991 (1990).
37. S. T. Chui and J. D. Weeks, *ibid.* **23**, 2438 (1981).
38. T. Jung, R. J. Phaneuf, E. D. Williams, unpublished results.
39. A. Saxena, T. Ala-Nissila, J. D. Gunton, *Surf. Sci.* **169**, L231 (1986), and references therein.
40. G. A. Somorjai and M. A. Van Hove, *Prog. Surf. Sci.* **30**, 201 (1989), and references therein.
41. The relation between the projected surface free energy f of Eq. 1 and γ is

$$f(\hat{n}_i) = \frac{\gamma(\hat{n}_i)}{\hat{n}_i \cdot \hat{n}}$$

where $\hat{n}$ is the surface normal of the reference surface.

42. J. W. Cahn, *J. Phys. Coll. C* **6** (suppl. 12), 199 (1982).
43. N. C. Bartelt, E. D. Williams, R. J. Phaneuf, Y. Yang, S. Das Sarma, *J. Vac. Sci. Technol. A* **7**, 1898 (1989).
44. P. Nozières, *J. Phys.* **50**, 2541 (1989).
45. R. J. Phaneuf, E. D. Williams, N. C. Bartelt, *Phys. Rev. B* **38**, 1984 (1988).
46. B. Z. Olshanetsky and S. A. Teys, *Surf. Sci.* **230**, 184 (1990).
47. N. A. Gjostein, *Acta Metall.* **11**, 969 (1963).
48. E. D. Williams and N. C. Bartelt, *Ultramicroscopy* **31**, 36 (1989).
49. J. Wei, N. C. Bartelt, E. D. Williams, in *The Structure of Solid Surfaces-III*, M. A. Van Hove, S. Y. Tong, X. Xie, K. Takayanagi, Eds. (Springer, Berlin, 1991).
50. H. P. Bonzel, in *Surface Mobilities on Solid Materials*, V. T. Bihn, Ed. (Plenum, New York, 1981), pp. 195–241.
51. J. M. Blakely and C. C. Umbach, in *Diffusion at Interfaces: Microscopic Concepts*, M. Grunze, H. Kreuzer, J. J. Weimer, Eds. (Springer, Berlin, 1988), pp. 102–120.
52. G. S. Bales and A. Zangwill, *Phys. Rev. B* **41**, 5500 (1990); G. S. Bales, A. C. Redfield, A. Zangwill, *Phys. Rev. Lett.* **62**, 776 (1989).
53. M. Kardar, G. Parisi, Y.-C. Zhang, *Phys. Rev. Lett.* **56**, 889 (1986).

54. We are grateful to T. L. Einstein, N. Gehrels, and M. G. Lagally for careful reading of the manuscript. This work has been supported by the Department of Defense and the National Science Foundation under grant number DMR-89-18829.